J. Fluid Mech. (1990), *vol.* 216, *pp.* 161–191
Printed in Great Britain

Numerical simulation of liquid-metal MHD flows in rectangular ducts

By A. STERL†

Association KfK-EURATOM, Kernforschungszentrum Karlsruhe, Institut für Reaktorbauelemente, Postfach 3640, D-7500 Karlsruhe 1, FRG

(Received 23 May 1989 and in revised form 14 December 1989)

To design self-cooled liquid metal blankets for fusion reactors, one must know about the behaviour of MHD flows at high Hartmann numbers. In this work, finite difference codes are used to investigate the influence of Hartmann number M, interaction parameter N, wall conductance ratio c, and changing magnetic field, respectively, on the flow.

As liquid-metal MHD flows are characterized by thin boundary layers, resolution of these layers is the limiting issue. Hartmann numbers up to 10^3 are reached in the two-dimensional case of fully developed flow, while in three-dimensional flows the limit is 10^2. However, the calculations reveal the main features of MHD flows at large M. They are governed by electric currents induced in the fluid. Knowing the paths of these currents makes it possible to predict the flow structure.

Results are shown for two-dimensional flows in a square duct at different Hartmann numbers and wall conductivities. While the Hartmann number governs the thickness of the boundary layers, the wall conductivities are responsible for the pressure losses and the structure of the flows. The most distinct feature is the side layers where the velocities can exceed those at the centre by orders of magnitude.

The three-dimensional results are also for a square duct. The main interest here is to investigate the redistribution of the fluid in a region where the magnetic field changes. Large axial currents are induced leading to the 'M-shaped' velocity profiles characteristic of MHD flow. So-called Flow Channel Inserts (FCI), of great interest in blanket design, are investigated. They serve to decouple the load carrying wall from the currents in the fluid. The calculations show that the FCI is indeed a suitable measure to reduce the pressure losses in the blanket.

1. Introduction

The flow of liquid metals in strong magnetic fields has been a topic of great interest in the past (e.g. Hunt 1965; Walker & Ludford 1974*a*, *b*, 1975; Hunt & Holroyd 1977; Holroyd & Walker 1978). Recently it came into consideration again in the framework of the development of a fusion reactor blanket (Carré *et al.* 1984; Smith *et al.* 1984). The so-called self-cooled liquid-metal blanket (Malang *et al.* 1988) uses liquid lithium or the eutectic alloy Pb-17Li as the coolant as well as the breeding material, thereby simplifying the mechanical design of the blanket.

However, the interaction between the moving conductor and the strong magnetic field confining the plasma induces electric currents, which in turn produce the

† Present address: Max-Planck-Institut für Meterologie, Bundesstrasse 55, D-2000 Hamburg 13, FRG.

Lorentz force $\boldsymbol{j} \times \boldsymbol{B}$ opposing the flow and creating large pressure losses. The Lorentz force is much larger than the frictional and inertial forces, which are confined to thin layers with rapid changes of velocity. Therefore, the velocity profiles of magnetohydrodynamic (MHD) flows in strong fields are quite different from those of ordinary hydrodynamic flows. This affects the heat and mass transfer. So to design self-cooled liquid-metal blankets, knowledge about MHD flows is needed.

The dimensionless parameter characterizing MHD flows is the Hartmann number M. It gives the ratio of Lorentz force to frictional force. The exact definition will be given in §2. In fusion blankets, M is in the order of 10^4 (Holroyd & Mitchell 1984).

MHD flows at large Hartmann numbers have been studied extensively by the method of asymptotic expansions. A review of the results of these studies is given by Walker (1986*a*). Asymptotic analysis is based on assumptions on the order of magnitude of different terms in the governing equations. Generally, inertia and friction are neglected. These kinds of assumptions can lead to results which are not valid for the parameters which are characteristic of the fusion blanket (cf. Talmage & Walker 1987). Therefore, semi-analytical or semi-numerical methods have been developed (Talmage & Walker 1987; Hua *et al.* 1988; Madarame & Hagiwara 1988; Tillack 1988) which overcome some of the restrictions of the asymptotic approach, but still are not able to describe the velocity profile near the walls of the duct correctly. They only give the volumetric flow rate in the vicinity of the walls. Furthermore, they break down in the outlet region of the magnet, or if the main flow direction and the magnetic field are parallel.

Hua & Picologlou (1989) show that the details of the velocity profile near the walls have little effect on the heat transfer, and Reed *et al.* (1987) found that the theoretical predictions are valid well into the regions of low magnetic field. Thus, from an engineering point of view, these restrictions seem to be of minor importance.

Nevertheless, the details of the flow are worth exploring. This can only be done by a fully numerical approach. This approach is difficult because of the thin layers in which inertia and friction are dominant, and which govern the structure of the flow. These layers must be resolved, which quickly leads to problems with storage or computing time. Therefore, only a small number of papers present analyses which use the fully numerical approach. Most of them consider one- or two-dimensional problems (e.g. one-dimensional: Wu 1973; two-dimensional: Winowich & Hughes 1982; Yagawa & Masuda 1982; Morozova, Nagornyi & Elkin 1983; Ramos & Winowich 1986). Ramos & Winowich (1986) report that they had problems with convergence at Hartmann numbers $M > 100$. Only a few groups of researchers dealt with three-dimensional problems. Khan & Davidson (1979) and Khan (1987) consider a parabolized form of the governing equations, whereas Aitov, Kalyntik & Tananaev (1983, 1984) and Kalis & Tsinober (1973) use the full set of equations. All groups restrict themselves to small Hartmann numbers ($M \leqslant 20$) because spatial resolution is limited by the storage available.

As computers have become more powerful, it is now possible to carry out fully numerical calculations at higher Hartmann numbers. The present work aims to explore the possibilities and limits of the fully numerical approach with present-day computers. Using a finite difference code, Hartmann numbers up to 10^3 for two-dimensional problems and up to 10^2 for three-dimensional problems are reached. Although these values are far below those occurring in fusion reactor blankets, the results presented reveal the principles of MHD flows at high Hartmann numbers.

The results are mainly consistent with those of earlier research, but provide more quantitative information since no assumptions about the order of magnitude of

several terms have to be made. Furthermore, results are obtained for the redistribution of flows parallel to a magnetic field, the behaviour of the flow in those regions at the inlet and outlet of a magnet where the field is weak, and of the importance of a streamwise component of the magnetic field.

2. Equations and boundary conditions

For liquid-metal MHD flows under fusion blanket conditions, the following assumptions are appropriate:

the fluid is incompressible, and;

the induced magnetic field $\boldsymbol{B}_{\text{ind}}$ is negligible compared to the imposed field $\boldsymbol{B}_0$.

Additionally we assume the flow to be isothermal, thus decoupling the energy equation from the momentum equations. Under these assumptions the governing equations, in dimensionless form, are (e.g. Walker 1981) as follows.

Conservation of mass

$$\operatorname{div} \boldsymbol{v} = 0, \tag{2.1}$$

conservation of momentum (Navier–Stokes equation)

$$\frac{1}{N}[\partial_t \boldsymbol{v} + (\boldsymbol{v}\cdot\nabla)\boldsymbol{v}] = -\nabla p + \boldsymbol{j}\times\boldsymbol{B} + \frac{1}{M^2}\nabla^2\boldsymbol{v}, \tag{2.2}$$

Ohm's law

$$\boldsymbol{j} = \boldsymbol{E} + \boldsymbol{v}\times\boldsymbol{B} = -\nabla\Phi + \boldsymbol{v}\times\boldsymbol{B}, \tag{2.3}$$

and Poisson's equation for the electric potential

$$\Delta\Phi = \operatorname{div}(\boldsymbol{v}\times\boldsymbol{B}) = \boldsymbol{B}\cdot\operatorname{curl}\boldsymbol{v}. \tag{2.4}$$

Here t, $\boldsymbol{v}$, $\boldsymbol{j}$, p and Φ are the dimensionless time, velocity, electric current density, pressure, and electric potential, respectively. They are made dimensionless by a/v_0, v_0, $\sigma v_0 B_0$, $\rho_0 v_0^2 N$, and $a v_0 B_0$, respectively, where a is a characteristic length (radius of a circular pipe or half the height of a rectangular duct), v_0 the average velocity, σ the fluid's conductivity and ρ_0 its density.

The Hartmann number M and the interaction parameter N are two important dimensionless parameters characterizing MHD flows. With μ being the viscosity of the fluid, they are given by the ratio of Lorentz force to frictional force,

$$M = aB_0(\sigma/\mu)^{\frac{1}{2}}$$

and the ratio of Lorentz force to inertial force

$$N = \sigma a B_0^2/\rho_0/v_0.$$

Typical values for fusion blankets are $M \approx 10^4$ and $N \approx 10^5$ (Holroyd & Mitchell 1984). From these large numbers it can easily be seen that friction and inertia play no role in most parts of the flow ('core') and are dominant only in thin layers with rapid changes of velocity. But since these layers separate the core regions from one another and from the walls, they determine the structure of the flow. Thus in general, the terms with M and N in (2.2) may not be discarded.

In addition to the governing equations, boundary conditions have to be specified. The walls of the ducts under consideration are impermeable and friction is present. So the condition on velocity $\boldsymbol{v}$ is

$$\boldsymbol{v}|_{\text{wall}} = 0. \tag{2.5}$$

As the induced electric potential Φ extends into the walls, in general Maxwell's

equations have to be solved in the walls, too. However, for the case of thin walls, defined by $t_w \ll a, t_w$ being the thickness of the wall, Walker (1981) derives an approximation permitting one to consider the fluid only. In that case the boundary condition on Φ at the fluid/wall interface reads

$$\partial_n \Phi|_{\text{wall}} = c\nabla^2_{\parallel} \Phi|_{\text{wall}}. \tag{2.6}$$

Here $\nabla^2_{\parallel} = \partial_r^2 + \partial_s^2$ is the tangential part of the Laplacian, where n, r and s are forming an orthogonal coordinate system with n pointing into the wall. $c = \sigma_w t_w/\sigma a$ is the wall conductance ratio, σ_w being the conductivity of the wall's material. c is a measure of the conductance of the wall compared to that of the fluid. Equation (2.6) is valid for constant c. If c varies, e.g. because of varying wall thickness, this equation has to be generalized. The derivation proceeds in the same way as that of Walker (1981), starting from the observation that in the thin wall the potential does not depend on n, but is a function of the tangential coordinates r and s only. The generalized boundary condition then reads (Sterl 1989)

$$\partial_n \Phi|_{\text{wall}} = [\nabla_{\parallel}(c\nabla_{\parallel} \Phi)]_{\text{wall}} = [c\nabla^2_{\parallel} \Phi + \nabla_{\parallel} c \nabla_{\parallel} \Phi]_{\text{wall}}. \tag{2.7}$$

Here $\nabla_{\parallel}$ is the tangential part of the gradient operator.

Equation (2.7) can be interpreted as follows (L. Bühler, private communication). As the potential of the wall does not depend on n, it is given by $\Phi|_{\text{wall}}$. The current density, integrated over the thickness of the wall, then is $-c\nabla_{\parallel}|_{\text{wall}}$. Its divergence, $-\nabla_{\parallel}(c\nabla_{\parallel} \Phi)|_{\text{wall}}$, must equal the amount of current which enters or leaves the wall. It is given by $-\partial_n \Phi|_{\text{wall}}$. Together, these expressions give (2.7) which therefore states nothing but the conservation of current at the fluid/wall interface.

3. Two-dimensional flow in a rectangular duct

3.1. *Formulation of the problem*

We first consider the problem of an infinitely long duct of rectangular cross-section (figure 1) which is placed in a homogeneous magnetic field

$$\boldsymbol{B}_0 = B_0(0, \sin\alpha, \cos\alpha) \quad (\text{dimensionless}: B_0 = 1). \tag{3.1}$$

As half the height of the duct is used as the lengthscale, the cross-section of the duct is $-1 \leqq y \leqq 1, -z_0 \leqq z \leqq z_0$. The magnetic field, the wall conductance ratio, and the cross-section are independent of x. Hunt (1969) shows that under these circumstances only one time-independent flow exists,

$$\begin{aligned} \boldsymbol{v} &= (u(y,z), 0, 0), \\ \Phi &= \Phi(y,z), \\ p &= p_0 - p_0' x, \quad -\operatorname{grad} p = (p_0', 0, 0). \end{aligned} \tag{3.2}$$

In addition to the influence of the magnetic field (strength and direction), we study the effect of the wall conductance ratio on the flow. To this end, the wall conductance ratios of the four walls (c_t (top), c_b (bottom), c_l (left), c_r (right)) can be chosen independently of one another.

Using the above-mentioned assumptions, the governing equations (2.1)–(2.4) reduce to a Poisson-type equation for the electric potential

$$\nabla_2^2 \Phi(y,z) = \mathrm{D}_x u(y,z), \tag{3.3a}$$

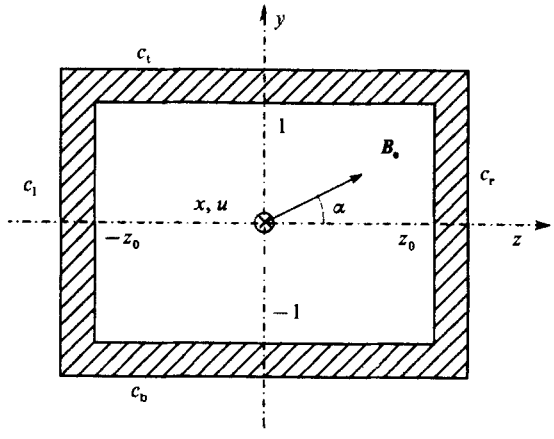

FIGURE 1. Rectangular duct in a homogeneous B-field.

and a Helmholtz-type equation for the velocity,

$$\nabla_2^2 u(y,z) - M^2 u(y,z) = -M^2(p_0' + \mathrm{D}_\alpha \Phi(y,z)). \tag{3.3b}$$

Here ∇_2^2 is the two-dimensional Laplacian,

$$\nabla_2^2 = \partial_y^2 + \partial_z^2, \tag{3.3c}$$

and

$$\mathrm{D}_\alpha = -\cos\alpha\,\partial_y + \sin\alpha\,\partial_z \tag{3.3d}$$

is a first-order differential operator depending on the direction α of the magnetic field. Via the right-hand sides of (3.3a, b), D_α is responsible for the coupling between the two unknowns Φ and u.

The boundary conditions (2.6) and (2.7) become

$$u(\pm 1, z) = u(y, \pm z_0) = 0, \tag{3.4}$$

$$\pm\partial_y \Phi(\pm 1, z) = \partial_z[c_{t,b}\,\partial_z \Phi(\pm 1, z)], \tag{3.5a}$$

$$\pm\partial_z \Phi(y, \pm z_0) = \partial_y[c_{r,l}\,\partial_y \Phi(y, \pm z_0)]. \tag{3.5b}$$

Hunt (1965) gives an analytical solution of the problem in the form of an infinite series for two special cases

(i) $$c_t = c_b = \infty, \quad c_l = c_r = \text{arbitrary},$$

(ii) $$c_t = c_b = \text{arbitrary}, \quad c_l = c_r = 0.$$

The series for case (ii) is computed to validate the program which numerically solves (3.3)–(3.5).

3.2. *Introduction of a wall-function* Φ_w

Solving of the Poisson- and Helmholtz-type equations (3.3) is done by the fast Poisson solver PWSCRT of Swarztrauber & Sweet (1975). It is capable of handling Dirichlet- and Neumann-type boundary conditions, but not a combination of first and second derivatives as in (2.7) or (3.5).

To handle this type of boundary condition, a wall function Φ_w is introduced (Walker, private communication) by a slight modification of (2.7)

$$\nabla_\parallel (c \nabla_\parallel \Phi_w^{(k+1)}) = \partial_n \Phi^{(k)}|_{\text{wall}}. \tag{3.6}$$

Here k is an iteration count. The right-hand side of (3.6) is calculated from the solution $\Phi^{(k)}$ of the kth iteration step. Then (3.6) is solved for $\Phi_w^{(k+1)}$, which in turn is used as a Dirichlet-type boundary condition on Φ in the $(k+1)$th iteration step. Clearly, (3.6) reduces to (2.7) when convergence is achieved.

Unfortunately, this algorithm proves to be unstable. This is due to the fact that c is a small parameter. Considering the special case of c = constant, we see that the right-hand side of (3.6) is multiplied by the large factor $1/c$. This factor amplifies the errors which are present in $\partial_n \Phi^{(k)}|_{\text{wall}}$ because it is only an approximation to the correct boundary value.

To overcome this problem an underrelaxation has to be performed. Let $\Phi_w^{*(k+1)}$ be the wall potential calculated from (3.6). Then instead of this, the following quantity is used as the boundary condition in the $(k+1)$th iteration step

$$\Phi_w^{(k+1)} = (1-\omega)\Phi_w^{(k)} + \omega \Phi_w^{*(k+1)}. \tag{3.7}$$

Empirically, the following value has been found appropriate for ω

$$\omega = \tfrac{1}{2}\min(c_t, c_b, c_l, c_r). \tag{3.8}$$

In general (3.6) has to be solved numerically. However, in the two-dimensional case of (3.5), it can be solved analytically. Consider the top wall of the duct. The corresponding equation for the top-wall potential Φ_t then reads

$$\partial_z[c_t(z)\,\partial_z \Phi_t^{(k+1)}(z)] = \partial_y \Phi^{(k)}(l, z). \tag{3.9}$$

Dropping k for convenience this can be integrated to give

$$\Phi_t(z) = \Phi_{t0} + \Phi'_{t0}\int_{-z_0}^{z} \frac{dz'}{c_t(z')} + \int_{-z_0}^{z} \frac{dz''}{c_t(z'')} \int_{-z_0}^{z''} dz' \partial_y \Phi(l, z'), \tag{3.10}$$

which can easily be calculated by the trapezoidal rule. Similar expressions hold for the other three walls. The eight integration constants Φ_{t0}, Φ'_{t0}, etc. are determined by additional constraints in the four corners of the cross-section which state that the potential is continuous and current is conserved. For the upper left corner $(-z_0, 1)$ they read

$$\Phi_t(-z_0) = \Phi_l(1), \tag{3.11a}$$

$$c_t\,\partial_z \Phi_t|_{z=-z_0} = c_l\,\partial_y \Phi_l|_{y=1}. \tag{3.11b}$$

To keep the resulting system determining the integration constants non-singular, the potential has to be fixed at some point, e.g.

$$\Phi_t(-z_0) = \Phi_0. \tag{3.12}$$

Physically this corresponds to a gauge of the potential.

3.3. *Performance of the code*

The two equations (3.3a) and (3.3b) are solved alternatively, thus forming an iteration process. This iteration can be combined with that for determining the correct boundary on Φ, as described in the previous section.

As PWSCRT is used, spatial discretization has to be done on a regularly spaced grid. This leads to some problems with storage capacity when going to high Hartmann numbers.

The higher the Hartmann number M, the thinner the boundary layers. The Hartmann layers at walls perpendicular to $\boldsymbol{B}$ scale with M^{-1}, and the side layers at walls parallel to $\boldsymbol{B}$ with $M^{-\frac{1}{2}}$ (e.g. Walker 1981). So to resolve these layers properly,

the grid spacing has to be reduced with growing M. Experience shows that at least 2–3 points within M^{-1} are necessary to obtain reasonable results, i.e. results lying within a few per cent of the correct values defined by Hunt's solution (cf. §3.1). This leads to at least 2400×2400 points for $M = 10^3$ which is beyond the capacity of the SIEMENS 7890 machine used in this research.

Fortunately, it is not necessary to use the same number of points in both coordinate directions. Consider the case $\alpha = 90°$, where D_α reduces to the z-derivative. It is then observed that the number of points in the z-direction is much more important than that in the y-direction. So calculations at $M = 100$ with 240×240 and 120×240 points yield the same results, whereas one with 240×120 differs significantly. The explanation is that the coupling between the u- and the Φ-equations is now dependent only on the z-direction, which therefore must be better resolved than the y-direction, even though the Hartmann layers, the thinnest layers occurring, form themselves at the y-boundaries! Therefore calculations for $M = 10^3$ are performed with only 120×1000 points.

The fact that the proper representation of the coupling between the two equations (3.3*a*) and (3.3*b*) is very important is stressed by another observation. Approximating the first derivatives in the operator D_α in fourth order instead of second order increases accuracy significantly. For example, for $M = 10^2$ and 240×240 points, the deviation from the exact (Hunt) result is about 10% for a second-order approximation, but only about 2% for fourth-order.

The number of iteration steps needed for convergence increases with rising Hartmann number and decreasing wall conductance ratio. The first dependence reflects the fact that gradients become steeper when M grows, while the second is a direct consequence of the underrelaxation needed, cf. (3.8). For example, with $M = 10^2, c_b = c_t = c_l = c_r = 5 \times 10^{-3}$ and 240×240 points, more than 1200 iterations are needed, leading to a computing time of about two hours on KfK's (Kernforschungszentrum Karlsruhe) SIEMENS 7890-machine.

3.4. *Results*

The results of the calculations are presented graphically by depicting current density and velocity. These results are confined to the special case of a square duct, i.e. $z_0 = 1$.

The current density is calculated from $u(y, z)$ and $\Phi(y, z)$ using Ohm's law (2.3). It is represented by arrows lying in the (y, z)-plane. Velocity is represented by a three-dimensional surface above the duct's cross-section. The distance between the surface and the (y, z)-plane corresponds to $u(y, z)$. Additionally, the values for u_{max}, the maximum velocity, dp/dx, the dimensionless pressure gradient, and α, the angle between the z-axis and $\boldsymbol{B}$ are given. Also the direction of $\boldsymbol{B}$ is represented by an arrow in every picture.

Pressure is made dimensionless with the interaction parameter N (cf. §2). As N is proportional to M^2, the dimensional pressure gradient $(dp/dx)^*$ is proportional to $M^2(dp/dx)$. This is important to remember when comparing values of dp/dx at different Hartmann numbers.

The basic phenomena of two-dimensional MHD flows will now be explained for the case $\alpha = 90°$ (figures 2 and 3). From the current density plots it can be seen that the current flows to the right-hand side in most of the duct's cross-section. This domain is known as the 'core' of the flow. Flow back to the left-hand side to close the circuit takes place only in narrow layers at the top and bottom walls. These are the Hartmann layers. Comparison of figures 2(*a*) and 2(*b*) shows that these layers become thinner as M increases. Finally, at the sidewalls, current flows mainly in the

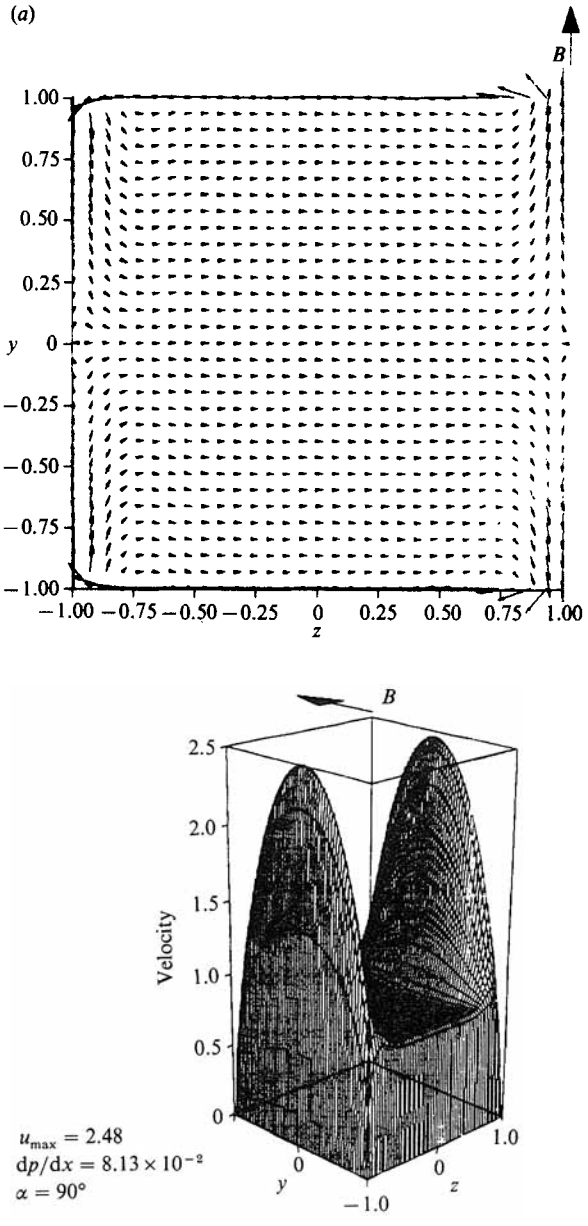

FIGURE 2(a). For caption see facing page.

y-direction. This is the region of the side layers. Comparing pictures for different wall conductance ratios (figures 2a, 3a, b) we see that the current density rises when the conductance ratio of the top and bottom walls (c_t, c_b) is increased, while the influence of the sidewalls' conductivity is much less. Obviously, the resistance of the Hartmann layers is the limiting value for the current flow. If another resistance, namely that of the top wall, is in parallel to that of the Hartmann layer, the total resistance is reduced and the current density is rising (cf. Picologlou 1985), thereby increasing the pressure gradient.

Looking at the velocities we easily find the three regions: core, Hartmann layer

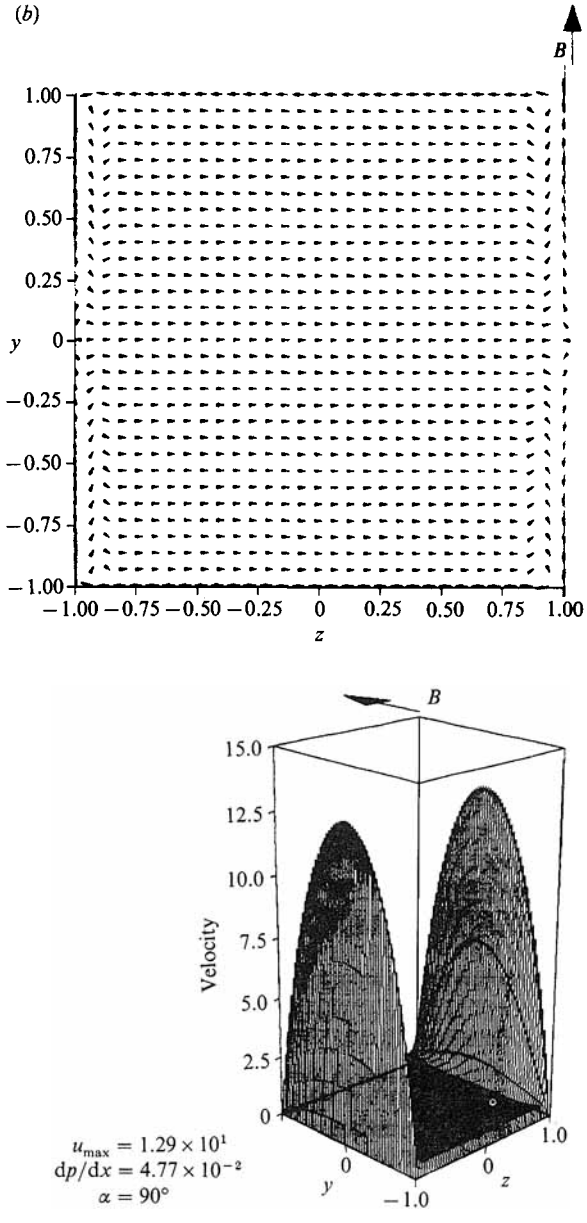

FIGURE 2. Current density (top) and velocity (bottom) in a duct with well-conducting top and bottom walls ($c_t = c_b = 0.1$) and non-conducting sidewalls at different Hartmann numbers (*a*) $M = 10^2$, (*b*) $M = 10^3$. The Hartmann and side layers can be distinguished clearly, becoming thinner as M grows.

and side layer again. In the core, the velocity is nearly constant, abruptly falling to zero in the thin Hartmann layers. The most interesting region, however, is the side layers. Their structure is strongly dependent on the wall conductance ratios and therefore on the current densities. The larger the current densities, the higher the velocities are in the side layers, forming the so-called M-shaped profiles.

The explanation of this striking phenomenon is straightforward (Hunt 1965). In the side layers the current density always has a component j_y parallel to $\boldsymbol{B}_0$. It does

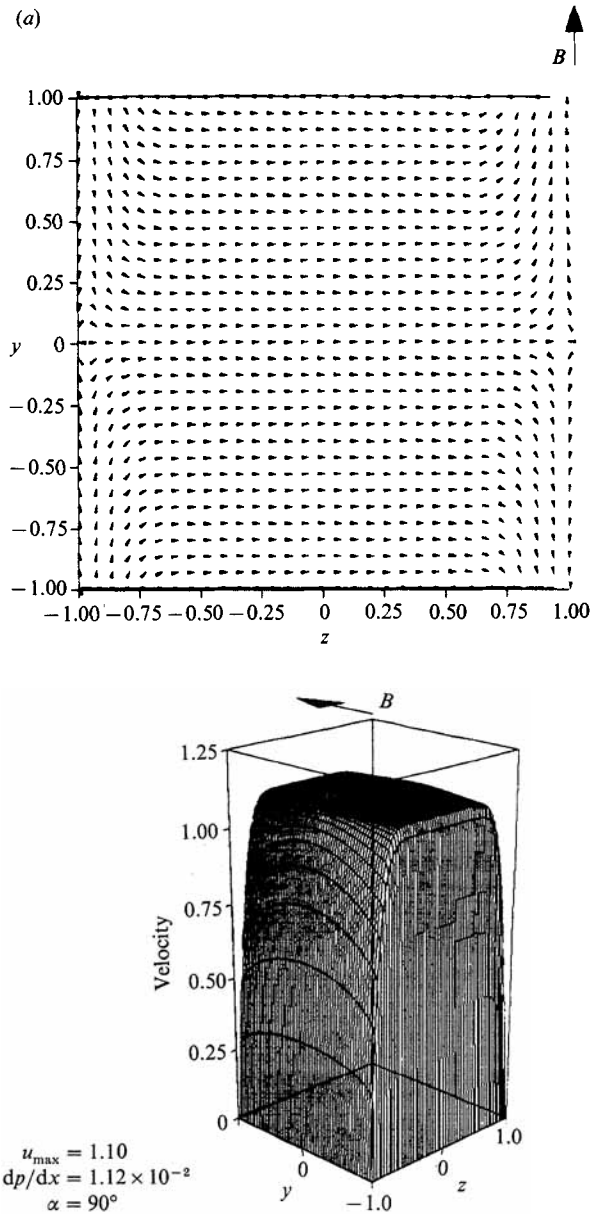

FIGURE 3(*a*). For caption see facing page.

not contribute to the Lorentz force $\boldsymbol{j} \times \boldsymbol{B}_0$ acting against the flow. On the other hand, in the core j_y vanishes, and the whole current contributes to $\boldsymbol{j} \times \boldsymbol{B}_0$ leading to a higher force. This can be seen clearly by comparing sidewalls with different conductivities. In figure 3(*b*) the right-hand sidewall is poorly conducting leading to a small z-component of $\boldsymbol{j}$. Therefore $\boldsymbol{j} \times \boldsymbol{B}_0$ is small, too, and the velocity is high. At the left, highly conducting side, the current has a comparatively large z-component, producing a large Lorentz force. Thus the velocity is reduced. This effect is more pronounced when the total current density is higher.

Figures 2 and 3(*b*) show a minimum of the velocity at the boundary between core

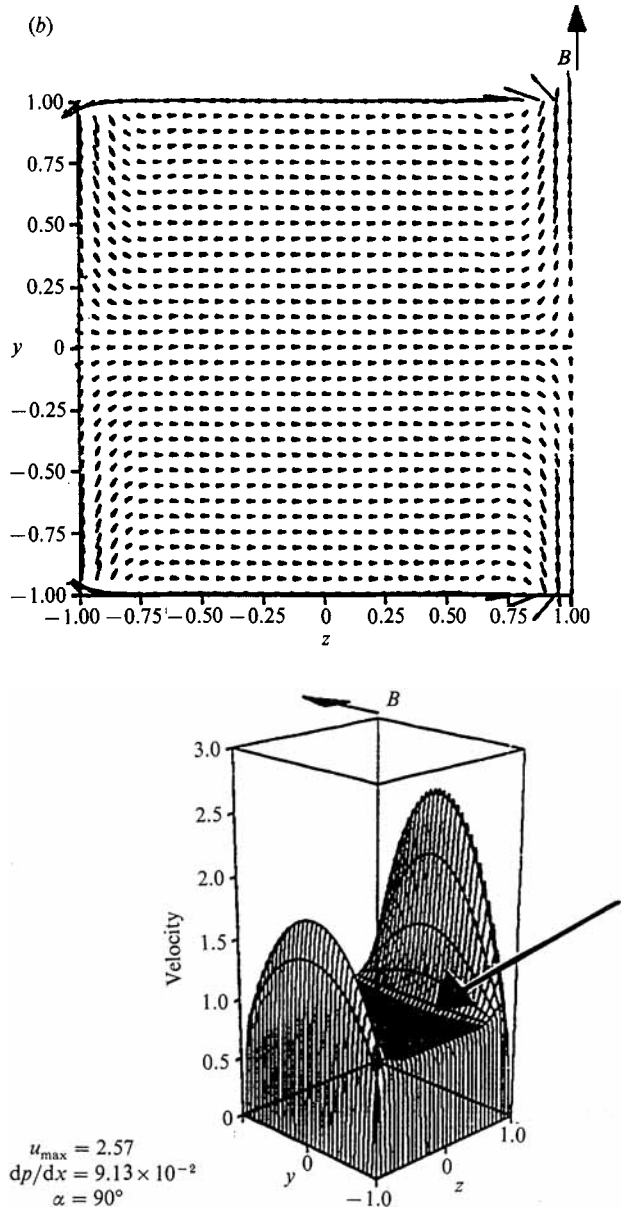

FIGURE 3. Current density (top) and velocity (bottom) at $M = 10^2$ for different wall conductance ratios. $\alpha = 90°$. (*a*) all walls non-conducting, (*b*) $c_t = c_b = c_i = 0.1, c_r = 5 \times 10^{-3}$. The arrow points at the minimum between core and side layer. Comparing figures 2(*a*) and 3(*a*, *b*) we see that the conductivities of the top and bottom walls govern the pressure loss while those of the sidewalls determine the structure of the side layers.

and side layer (see arrow in figure 3*b*). Hunt (1965) shows that this minimum can even assume negative values. He gives a critical Hartmann number of $M_c = 89$ at $c_b = c_t = \infty$ (but cf. Temperly 1984, where $M_c = 96.3$). As only finite values for $c_{t,b}$ can be used in the code used here, this limit is not found. All flows considered with $M = 10^2$ exhibit no counter flow. At $M = 10^3$ and $c_t = c_b = 1$, however, negative

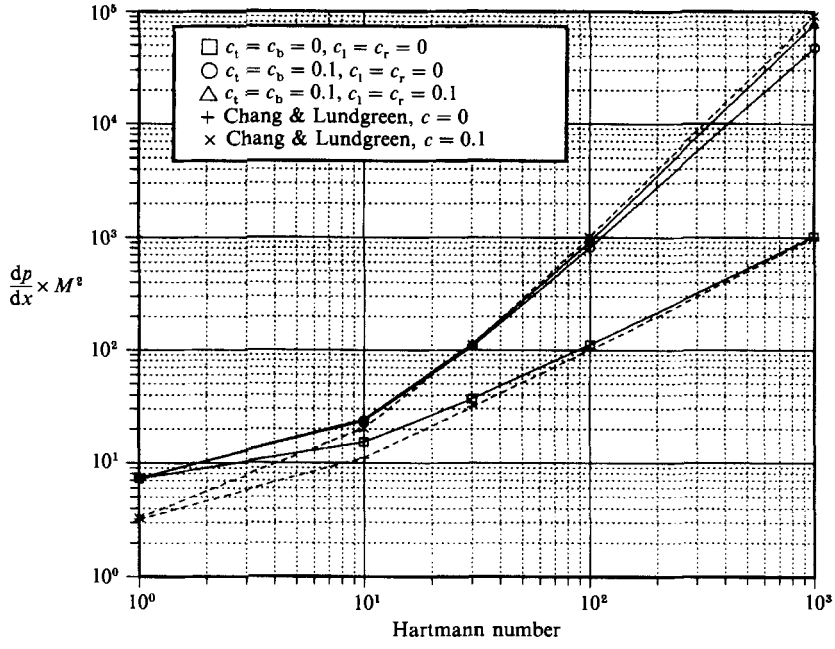

FIGURE 4. Pressure losses as a function of Hartmann number at different combinations of wall conductance ratios. The factor M^2 serves to make values for different M comparable as explained in the text. For comparison the curves resulting from the formula of Chang & Lundgren (1961) are also given.

values of velocity are found. It is possible, that the occurrence of negative velocities is only artificial. First, the assumption of a two-dimensional flow may not be valid at such high Hartmann numbers. Secondly, the resolution used (120×1000 points) may still be too coarse. Unfortunately, it is neither possible to carry out a three-dimensional calculation of the flow at $M = 10^3$ (cf. §4) nor to increase the resolution, so that the question remains open.

Figure 4 shows the dependence of $M^2(\mathrm{d}p/\mathrm{d}x)$ (which is proportional to the dimensional pressure gradient as explained above) on Hartmann number. At small Hartmann numbers, the influence of the wall conductance ratios is small, indicating that the electromagnetic influence on the flow is small. With M growing, MHD effects gain influence and the wall conductance ratios become important, the top and bottom walls playing the main role (see above). That is the reason why the formula for pressure losses derived by Chang & Lundgren (1961) for a channel with no sidewalls, is suitable for predicting the pressure loss in a duct. The Chang & Lundgren values are also plotted in figure 4 for comparison.

Investigating the influence of the direction of $\boldsymbol{B}_0$, it is seen that rotation of $\boldsymbol{B}_0$ causes a corresponding rotation of the velocity profile (figure 5). In addition, the wall conductance ratios of the top and bottom walls ($c_t = c_b = 0.1$) and those of the sidewalls ($c_l = c_r = 5 \times 10^{-3}$) are different. Thus they change roles during rotation, again showing the different influences of walls parallel and perpendicular to the magnetic field.

As can be seen from figure 4, the pressure loss rises if the wall conductance ratio rises. For technical applications in a blanket, it is therefore desirable to have c as low as possible, $c = 0$ being the optimum. Unfortunately, no known insulating material

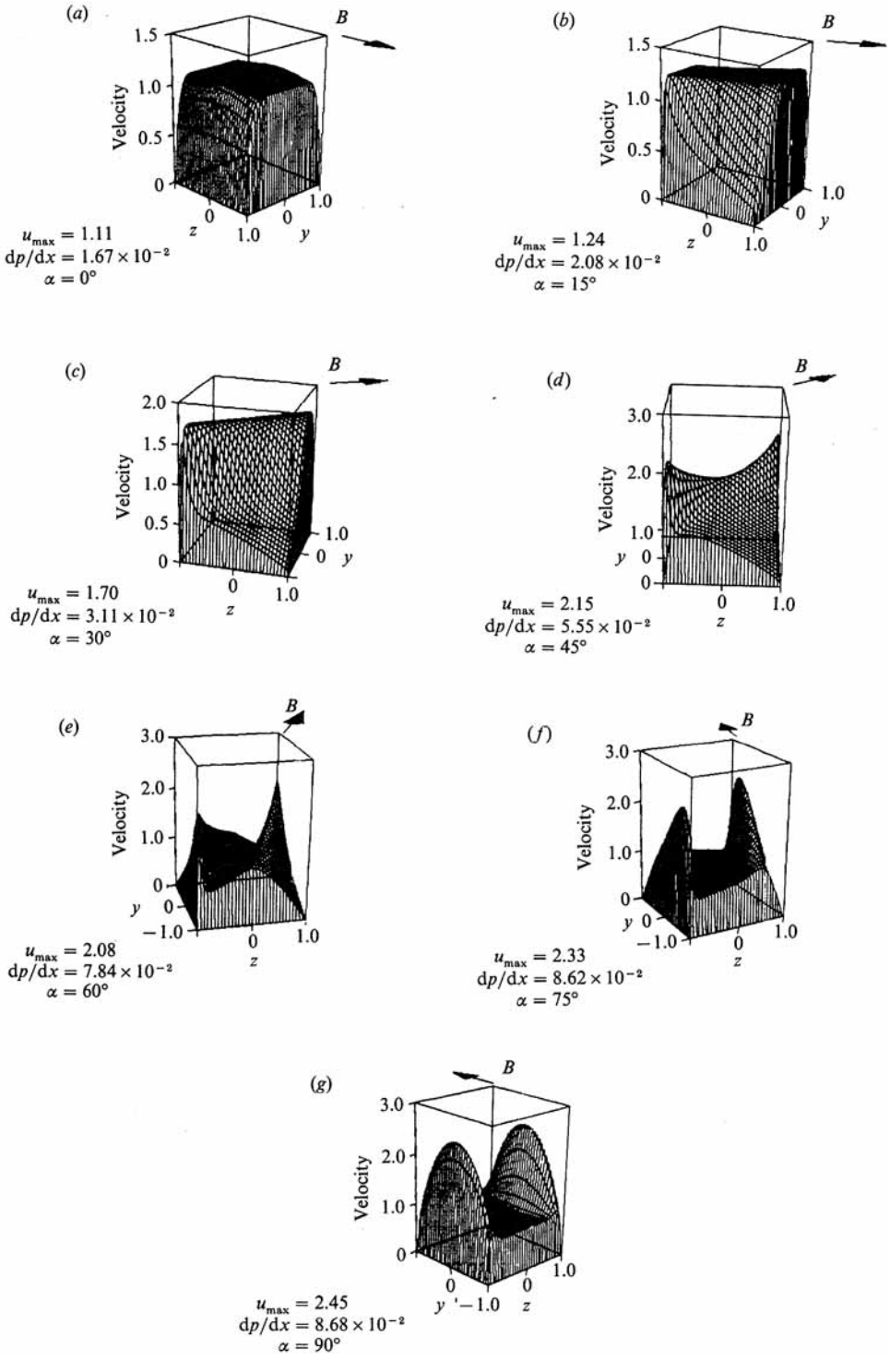

FIGURE 5. Velocity profiles for different directions of the magnetic field $\boldsymbol{B}_0$ at $M = 10^2$. As the conductances of the two pairs of walls are different ($c_t = c_b = 0.1$, $c_l = c_r = 10^{-3}$) they interchange their role during rotation. The different influence of walls perpendicular and parallel to $\boldsymbol{B}_0$ on the flow is thus revealed.

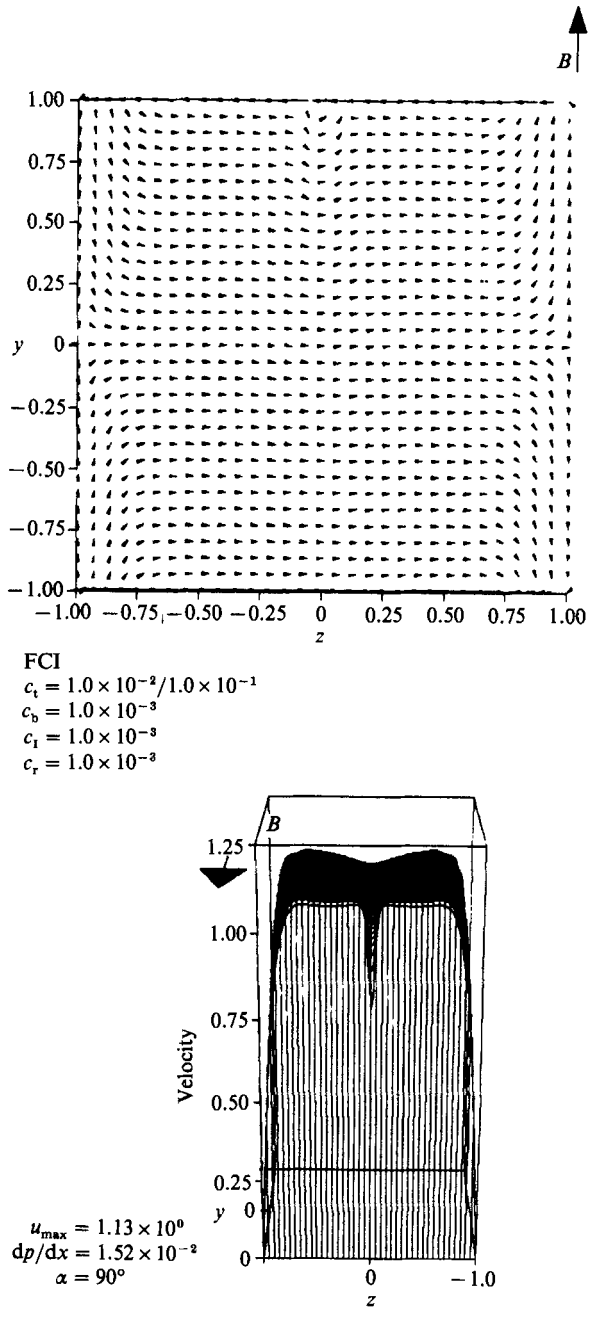

FIGURE 6. Current density (top) and velocity (bottom) at $M = 10^2$ in a duct whose wall conductivities simulate an FCI. The part of high conductance ($c = 0.1$) is situated at the middle of the top wall at $|z| \leqq 0.02$. There, a current vortex is formed leading to a notch in the velocity profile.

is compatible with liquid lithium at some hundred degrees. Thus one has to use conducting material for the wall, which may lead to unpermissibly high pressure losses (Malang *et al.* 1988).

To decouple the load carrying wall from the electric circuit induced in the fluid, the use of novel 'Flow Channel Inserts' (FCI) has been proposed (Malang *et al.* 1988).

FCIs are prefabricated units fitted loosely into the flow channels. They consist of a composite sheet with a ceramic layer sandwiched between two steel sheets. Mechanical stresses in the FCI become insignificant by providing a longitudinal slot for pressure equalization between the inner flow region and the outer gap.

The slot is filled with liquid metal. From the electrical point of view it forms a strip of good conductance in an otherwise poorly conducting wall. To investigate its influence we consider a duct of low wall conductance ratio ($c = 10^{-3}$), with a strip of good conductance ($c = 0.1$ for $|z| \leqq 0.02$) at the top wall. For the case of the slot being at a wall perpendicular to $\boldsymbol{B}_0$, the result is shown in figure 6. A current vortex forms in the close neighbourhood of the well conducting strip, leading to a small notch in the velocity profile. The reason for this is clear. The potential difference between $z = +0.02$ and $z = -0.02$ can drive a large current through the well conducting part of the top wall. This current cannot continue through the neighbouring poorly conducting parts of the wall, and therefore must close through the liquid, thereby forming the vortex. The Lorentz force produced by this current vortex causes the notch in the velocity profile.

If the slot is at a wall parallel to the magnetic field (not shown), it has no influence on the flow. This is due to the fact that no potential difference is induced on walls parallel to the magnetic field across the plane of symmetry, where the slot is placed. So there is no reason for additional currents to flow. Thus positioning the FCI with the slot across the plane of symmetry at a wall parallel to $\boldsymbol{B}_0$, the flow behaves as if all the walls were poorly conducting.

However, even in the case of having the FCI wrongly adjusted the influence of the slot is only small: the dimensionless pressure gradient rises only from 1.51×10^{-2} to 1.52×10^{-2}.

The results of the calculations compare well with those of Sezgin (1987), who considers insulated ducts with a strip of good conductance using a semi-analytical approach. A quantitative comparison between his results and those presented here is not possible, however, because the Poisson solver PWSCRT does not permit Neumann and Dirichlet boundary conditions arising from the isolated wall and the conducting strip, respectively, at the same wall.

Alty (1971) studies MHD flows in ducts in which one pair of opposite walls is designed as electrodes. Electrodes are characterized by a constant potential, a condition that is easily implemented into the code. The results of the numerical calculations mainly agree well with those of Alty. Only in one case is there a discrepancy. If the sidewalls are two short-circuited electrodes and the angle between the z-axis and the magnetic field is less than 45°, Alty finds two thin velocity jets situated parallel to the field. They extend over the whole duct from one corner to the opposite wall. The numerical simulation also shows these jets emanating from the corners (figure 7), but they do not reach the opposite walls. The reason for this is that Alty *a priori* considered the variables to be constant along the field lines. This assumption is obviously not correct.

4. Three-dimensional flows in a rectangular duct

4.1. *Description of the problem*

Up to now, the flows considered involve parameters (such as c, M, or the duct's cross-section) which are constant in the x-direction. In real applications, however, there will be gradients of $\boldsymbol{B}$, ducts of different wall conductance ratios welded together, changes in cross-section, or bends in the duct. All these items will produce deviations

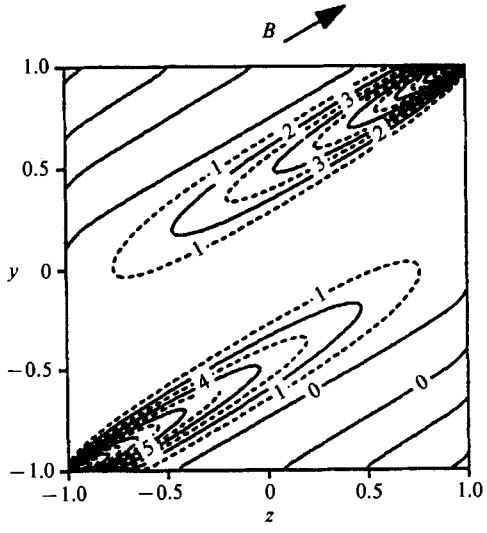

FIGURE 7. Isotachs in a duct with short-circuited sidewalls, $M = 200$ and $\alpha = 30°$. In contrast to the results of Alty (1971), the regions of high velocity do not reach the opposite wall.

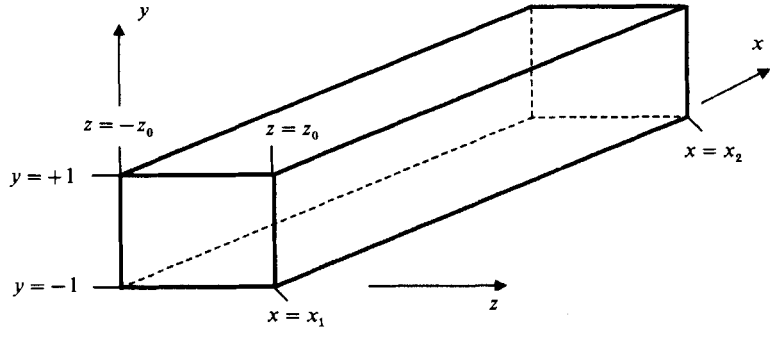

FIGURE 8. Geometry considered for three-dimensional calculations.

from fully developed two-dimensional flow, leading to interesting three-dimensional effects, some of which have been studied analytically (e.g. Walker & Ludford 1974*a*, *b*, 1975; Walker 1986*a–e*).

This research is confined to three-dimensional effects caused by variations of the magnetic field or the wall conductance ratio along x. Changes in the geometry of the duct will not be considered, thus avoiding numerical problems arising from computational domains whose boundaries are not parallel to the coordinate directions. For such domains efficient Poisson solvers are not known. In the case considered here, the computational domain is rectangular (figure 8), a case for which efficient solvers are available. Here, a program is used that was kindly provided by Dr Schumann (DLR, Oberpfaffenhofen). It uses FFT methods described in Schumann & Sweet (1988) and incorporates staggered boundary conditions.

Three-dimensional effects are introduced by changes in the magnetic field $\boldsymbol{B}_0$ or the conductance ratios of the walls, which may be any desired function of the coordinates,

$$\boldsymbol{B} = (B_x(x,y,z), B_y(x,y,z), B_z(x,y,z)), \tag{4.1}$$

$$\left.\begin{aligned} z = -z_0\colon\ & c_\mathrm{l} = c_\mathrm{l}(x,y), \quad z = z_0\colon\ c_\mathrm{r} = c_\mathrm{r}(x,y), \\ y = -1\colon\ & c_\mathrm{b} = c_\mathrm{b}(x,z), \quad y = 1\colon\ c_\mathrm{t} = c_\mathrm{t}(x,y). \end{aligned}\right\} \tag{4.2}$$

The entrance and exit are at x_1 and x_2, respectively. Boundary conditions at these cross-sections are not known exactly unless they are so far away from the three-dimensional region that the flow is fully developed. Therefore x_1 and x_2 have to be chosen such that they are not too close to the three-dimensional region, but as close to it as possible to prevent the computational domain from becoming too large.

To solve the problem, the full set of MHD equations (2.1)–(2.4) has to be used, along with boundary conditions (2.5) and (2.7) at the walls. They have to be supplemented by boundary conditions at the entrance and exit. As already mentioned, the entrance and exit are in regions of fully developed flow. These are characterized by

$$\partial_x u = \partial_x \Phi = v = w = 0, \tag{4.3}$$

which is used as the boundary condition. If the entrance or exit is outside the magnetic field, $\Phi = 0$ may be specified there. It is also possible to specify u at the entrance instead of putting $\partial_x u = 0$ there.

Pressure is fixed at inlet and outlet. Care has to be taken to ensure that the average dimensionless velocity assumes a value of one. This is necessary because the average velocity v_0 has been used to non-dimensionalize all quantities (cf. §2). The boundary conditions for pressure at the walls will be explained in the next section.

4.2. *Description of the algorithm*

The system of equations (2.1)–(2.4) is solved for steady state. To arrive there, the Navier–Stokes equation (2.2) is advanced forward in time by an ADI method described below. At each timestep, two Poisson-type equations for pressure and electric potential are solved. The equation for potential is given by (2.4), whereas that for pressure is derived from a time-splitting method due to Kim & Moin (1985). In this method, (2.2) is integrated without the pressure term, resulting in an intermediate velocity $\boldsymbol{v}'$. Then $p^{(n+1)}$, the superscript denoting the timestep, is calculated so as to fulfil (2.1), leading to

$$\Delta p^{(n+1)} = \frac{1}{\Delta t} \operatorname{div} \boldsymbol{v}', \tag{4.4}$$

where Δt is the time increment. $p^{(n+1)}$ is then used to update $\boldsymbol{v}'$ to get the final $\boldsymbol{v}^{(n+1)}$

$$\boldsymbol{v}^{(n+1)} = v' - \Delta t \cdot \nabla p^{(n+1)}, \tag{4.5}$$

which by construction is divergence-free.

To be compatible with (2.5), the boundary condition on p at the walls must be

$$\partial_n p\,|_{\text{wall}} = 0, \tag{4.6}$$

where the subscript n denotes the normal derivative.

The ADI method is used in the following way. The Navier–Stokes equation (2.2) is written in the following form

$$\partial_t \boldsymbol{v} = \mathrm{D}_x \boldsymbol{v} + \mathrm{D}_y \boldsymbol{v} + \mathrm{D}_z \boldsymbol{v} + \boldsymbol{R}. \tag{4.7}$$

Here $\mathrm{D}_x \boldsymbol{v}$ stands for the elliptic terms, namely

$$\mathrm{D}_x \boldsymbol{v} = \frac{N}{M^2} \partial_x^2 \boldsymbol{v}. \tag{4.8}$$

D_y and D_z are defined analogously, while $\boldsymbol{R}$ contains the remaining terms. The ADI algorithm used then reads (Douglas & Gunn 1964; Briley & McDonald 1980)

$$(1-\Delta t\, D_x)\, \boldsymbol{v}_1 = \Delta t[(D_x+D_y+D_z)\, \boldsymbol{v}^{(n)} + \boldsymbol{R}^{(n)}], \tag{4.9a}$$

$$(1-\Delta t\, D_y)\, \boldsymbol{v}_2 = \boldsymbol{v}_1, \tag{4.9b}$$

$$(1-\Delta t\, D_z)\, \boldsymbol{v}_3 = \boldsymbol{v}_2, \tag{4.9c}$$

$$\boldsymbol{v}^{(n+1)} = \boldsymbol{v}^{(n)} + \boldsymbol{v}_3. \tag{4.9d}$$

The ADI method described is stable as long as only the diffusive terms are considered. However, the convective stability limit given by the well-known CFL-condition has to be obeyed.

Spatial discretization is done on a staggered grid with p and Φ being defined at the centre of a cell, while the vector components are defined on the corresponding faces of the cell (e.g. Anderson, Tannehill & Pletcher 1984, p. 459). The derivatives are then approximated by the standard second-order central difference formulae. If values are needed where they are not defined, e.g. a velocity component at the cell's centre, they are linearly interpolated between adjacent points. Thus no upwind or donor-cell differentiation to stabilize the calculation is done. It is not necessary since due to the large interaction parameter, convection does not play an important role.

As in the two-dimensional case, a wall function Φ_w is introduced to incorporate the boundary condition (2.7) on Φ into the calculation (cf. §3.2). The defining equation (3.6), however, now has to be solved numerically. It is discretized in the usual way on an (x, s)-plane formed by unrolling the walls of the duct, s being the circumferential coordinate. Along the edges of the duct, compatibility conditions analogous to (3.11) have to be formulated. While (3.11a) which states that the potential is continuous at the edges remains unchanged, there is a change in (3.11b) which gives conservation of current. While in the two-dimensional case current can only flow from the left to the top wall, say, it is now able to flow in the x-direction, i.e. parallel to the edge, too. These currents have to be added to (3.11b) to get the correct condition on current conservation. The linear system obtained from discretizing (3.6) and the corresponding conditions at the edges is solved by the routine MA28AD/CD from the HARWELL subroutine library.

More details of the algorithm can be found in Sterl (1989).

4.3. *Performance of the code*

A computer program, MHD3D, incorporating the algorithm described above is implemented on KfK's scalar SIEMENS 7890 machine. Computation starts from an initial guess and is finished if the maximum relative changes in the velocities are less than 10^{-4}. The number of timesteps necessary does not depend on the number of grid points, but on the parameters M, N, c, and the gradient of $\boldsymbol{B}_0$. The higher M and the B-field gradient, the higher the number of timesteps needed, whereas less steps are needed if N or c increase. The dependence on M and c is thus the same as in the two-dimensional case (cf. §3.3).

The computation time per timestep is roughly proportional to the number of grid points used. For example, for 32^3 points, the usual resolution, it is 4.56 seconds, leading to large CPU-times. So for $M = 50$, $N = 10^3$, $c_t = c_b = 0.1$, $c_l = c_r = 10^{-3}$ and $x_0 = 0.15$ (definition of x_0 see below, (4.11)), 3020 timesteps are needed, leading to approximately 4 hours of CPU-time.

A maximum of 40×40 points is used in the cross-sectional plane. Based on the

discussion on the resolution needed in the two-dimensional case (cf. §3.3), it seems impossible to handle Hartmann numbers greater than about 30. However, the following observations are made.

(i) Calculations done with 32^3 points and $24\times40\times40$ points at $M = 10^2$ show differences of less than 5%.

(ii) In regions of fully developed MHD flow, the deviations from the corresponding two-dimensional calculations are at most 10% for the cases presented here.

(iii) The strength of the three-dimensional effects increases monotonically with increasing M.

(iv) Thus results obtained at high Hartmann numbers are at least qualitatively correct with respect to flows at higher M.

Therefore it is valid to conclude that the results presented for M up to 10^2 show the correct behaviour and are suited to gain insight into the physics and the phenomena of high Hartmann number MHD flows.

4.4. *Results*

4.4.1. *Preliminary remarks*

As mentioned earlier, two sources for three-dimensional effects are considered, namely changes in $\boldsymbol{B}_0$ or c along the flow direction. It is found that changes in $\boldsymbol{B}_0$ produce the most severe and spectacular effects, whereas changes in the wall conductance ratio have only minor implications. Therefore an extensive discussion of the influence of $\boldsymbol{B}_0$ changing in the streamwise direction is presented first. As in the two-dimensional case, the analysis is confined to a square duct.

The applied magnetic field is chosen to be

$$B_y(x) = \frac{1}{1+\mathrm{e}^{-x/x_0}}, \tag{4.10}$$

the other two components being set to zero to save computing time. If x_0 is positive, B_y rises from zero to one, while negative x_0 causes a corresponding decrease. The magnitude of x_0 governs the gradient of the field. Calculations are usually done with $x_0 = \pm 0.15$, giving rise to a rather steep gradient. The reason for choosing this value is to keep the streamwise extension of the computational domain as small as possible in order to obtain good resolution.

Unfortunately, the form (4.10) for the magnetic field is unphysical because it is not curl-free. As we want to avoid the complications of calculating a real, divergence- and curl-free field which necessitates solving an additional Poisson-type equation, we make additional calculations with the field

$$\boldsymbol{B}_0 = (y\,\partial_x B_y(x), B_y(x), 0), \tag{4.11}$$

(B_y from (4.10)), which is curl-free but not divergence-free. Therefore (4.11) only yields an estimate of the influence of neglecting B_x.

Comparison between results from calculations with and without a x-component of $\boldsymbol{B}_0$ shows that:

(i) the pressure drop is reduced using (4.11);

(ii) with (4.11), less fluid is driven into the side layers in the region where $\boldsymbol{B}_0$ changes.

These observations can easily be explained. As B_x opposes motion in z-direction, less fluid can flow to the sides. As a result, the redistribution of the velocity is reduced, which in turn reduces the pressure drop.

However, the differences between calculations with (4.10) and (4.11), respectively, are reasonably small so as to justify the use of the simple field (4.10). This is in accordance with arguments given by Talmage & Walker (1987).

4.4.2. *Flow entering B-field region – qualitatively*

The case with $M = 50, N = 10^3, c = 0.1$, and $x_0 = 0.15$ is chosen to be the reference case. The influence of the parameters will then be investigated by changing one of them while fixing the others.

Figure 9 shows the redistribution of the velocity profile. At different positions x along the duct, the u-velocity is plotted as a three-dimensional surface above the cross-section of the duct. For convenience, the field strength B_y is displayed, too. The first picture ($x = -2.13$) is far away from the magnetic field region ($B_y = 0$). This can easily be seen from the purely hydrodynamic profile. The second picture ($x = -1.13$) is situated right at the beginning of the field ($B_y = 5 \times 10^{-4}$). As a first consequence the Hartmann layers begin to evolve, resulting in a flattening of the profile parallel to the top and bottom walls. The next picture ($x = -0.63, B_y = 1.5 \times 10^{-2}$) shows the beginning of the M-shaped profile. The fluid is driven towards the side walls parallel to $\boldsymbol{B}_0$. In the following pictures the M-shape grows, reaching its maximum at $x = 0$. Here the B-field gradient has its maximum, also. Having passed the maximum, the M-shape decays into the fully developed MHD profile already known from §3. This final stage is shown in the last picture ($x = 2.13$, $B_y = 1$). While the profile in the z-direction passes through several intermediate states until the fully developed MHD profile is reached, the Hartmann layers, once formed, show no significant changes, their steep gradients remaining right next to the walls.

The transition from the fully developed hydrodynamic to the fully developed magnetohydrodynamic state thus is not monotonic, but passes through several intermediate states. They are highly M-shaped with nearly the whole mass flux carried by the side layers. What causes these intermediate states? To answer this question figure 10 is examined. Here the current density in the midplane perpendicular to $\boldsymbol{B}_0$ is shown. As the induced voltage across the duct parallel to z is proportional to $\boldsymbol{B}_0$, a streamwise potential gradient occurs leading to streamwise currents. As can be seen from figure 10, these currents close upstream and downstream of the variable field region. The Lorentz force associated with them accelerates the flow in the upstream region and decelerates it downstream. However, $\boldsymbol{B}_0$ and thus $\boldsymbol{j} \times \boldsymbol{B}_0$ are greater behind than before the transition region, thus leading to a net force opposing the fluid (cf. also Hunt & Holroyd 1977; Holroyd & Walker 1978).

Near the wall the currents are flowing in the x-direction producing no streamwise forces. Thus the Lorentz forces associated with the streamwise currents act as a kind of blockage of the central part of the duct. The fluid bypasses this blockage by flowing in the regions near the wall where the anti-streamwise force is low. However, the Lorentz forces in this region are directed towards the centre of the duct opposing the motion into the side-layers. The forces are balanced by a corresponding transverse pressure gradient, as can be seen from figure 11 in the next section.

4.4.3. *Flow entering B-field region – quantitatively*

Having discussed the phenomena occurring in the region of varying magnetic field, characteristic quantities are now defined which will be used to compare flows with different values of the parameters M, N, c, and x_0. For the standard case they are

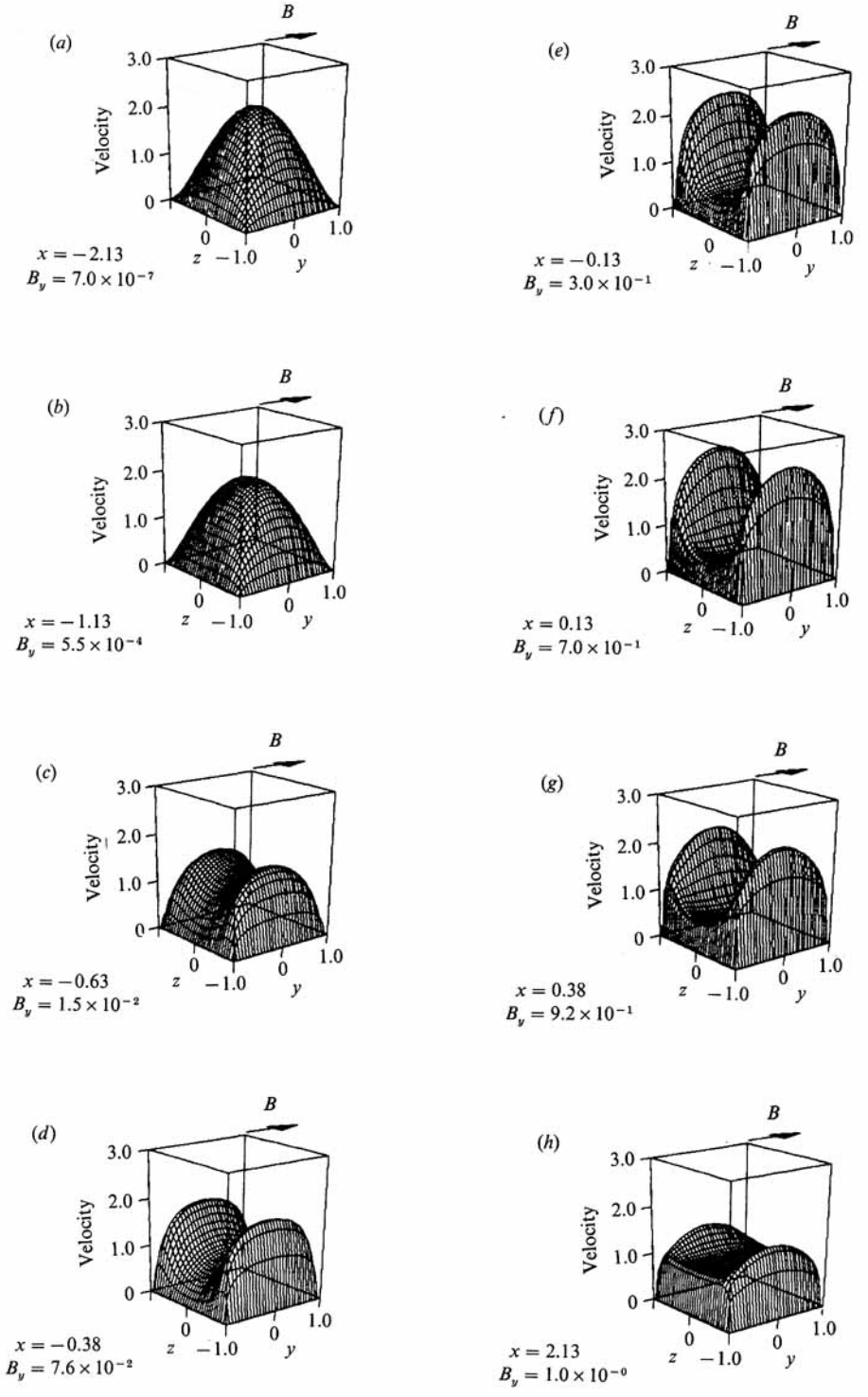

FIGURE 9. Profiles of u-velocity in the entrance region of a magnet at different cross-sections for the standard case. Starting from fully developed hydrodynamic flow the velocity is redistributed in the transition region, the fluid being driven towards the sidewalls. The evolving M-shaped profile then decays into the fully developed MHD profile.

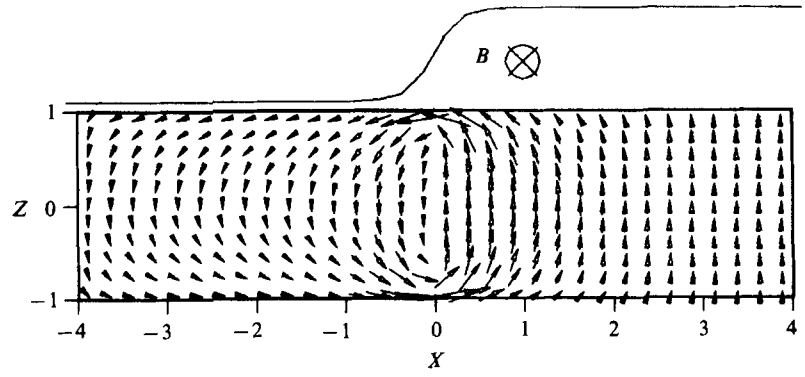

FIGURE 10. Axial currents induced in the region of varying magnetic field in the plane $y = 0$. The strength of the field is indicated by the upper curve.

shown in figure 11. They consist of:

the magnetic field $B_y(x)$ for the sake of orientation,
the pressure on the centreline, $p(x, 0, 0)$,
the pressure at the sidewall, $p(x, 0, 1)$,
the streamwise pressure gradient on the centreline, $-\partial_x p(x, 0, 0)$,
the centre of u-distribution at $y = 0$,

$$z_s(x) = \frac{\int_0^1 zu(x, 0, z)\,\mathrm{d}z}{\int_0^1 u(x, 0, z)\,\mathrm{d}z}, \tag{4.12}$$

the transverse potential difference,

$$\Delta\Phi_t(x) = |\Phi(x, 1, 0) - \Phi(x, 0, 1)|. \tag{4.13}$$

The centre of u-distribution is a measure of the 'M-shapedness'. The greater z_s, the greater the velocity in the side layers. For a purely hydrodynamic flow in a square duct, $z_s = 0.383$. A plug-type profile (u = constant) would yield $z_s = 0.5$. Thus if $z_s > 0.5$, the velocity is higher near the sidewalls than at the centre.

The corresponding curve of figure 11 clearly shows how the fluid is first driven towards the sides in the transition region, then comes back partly to form the fully developed MHD-profile which still has a slight M-form, as indicated by $z_s = 0.53$. This compares well with the last picture of figure 9.

Looking at the pressures next, it is clear that in the transition region the pressure at the centreline exceeds that at the wall. Thus there is a pressure gradient between wall and centre balancing the Lorentz force, as mentioned previously. In the regions of fully developed flow, this transverse pressure gradient is of course zero.

At the entrance, in the region of fully developed hydrodynamic flow the pressure gradient $-\partial_x p(x, 0, 0)$ is constant. At the beginning of the magnetic field it decreases a little, due to the Lorentz force accelerating the flow as discussed above. The pressure gradient then rises sharply, as now the Lorentz force caused by the closing streamwise currents opposes the flow. At the exit the gradient is somewhat lower, now being governed only by the currents induced in the cross-sectional plane as explained in §3.

The last curve gives the transverse potential difference $\Delta\Phi_t$ which can easily be measured. It is monotonically increasing. In fully developed MHD flows, $\Delta\Phi_t$ is

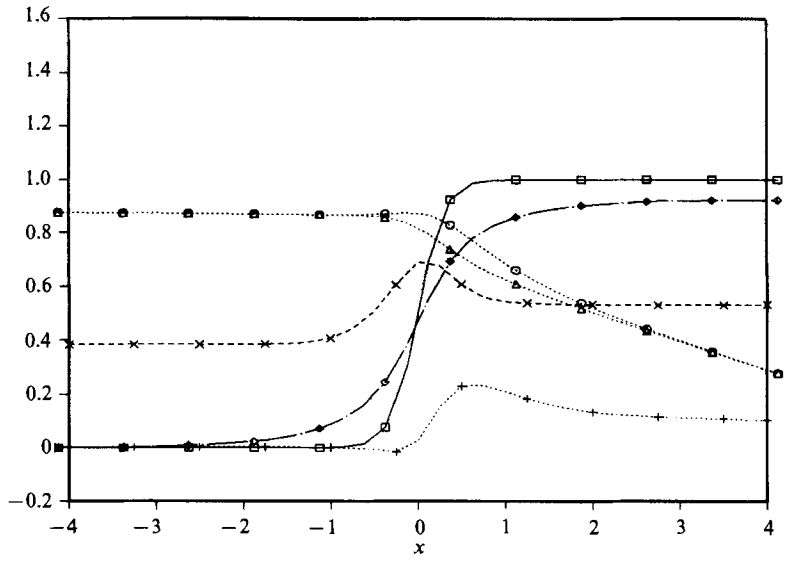

FIGURE 11. 'Characteristic quantities' as a function of streamwise position x for the standard case. The three-dimensional effects in the transition region can be seen clearly. □, magnetic field; ○, pressure at centre; △, pressure at side; +, pressure gradient; ×, centre of u-distribution; ◇, transverse potential difference.

proportional to $\boldsymbol{B}_0$. The difference between the slopes of the B_y-curve and the $\Delta\Phi_t$-curve is caused by the axial currents. They smear the potential distribution over a larger region.

4.4.4. *Influence of external parameters*

Figure 12 shows the influence of M on some quantities describing the three-dimensional effects. For comparison, the lowest curve shows the centre of u-distribution for fully developed hydrodynamic flow, which of course is independent of M. The next curve shows the centre of u-distribution for fully developed MHD flow. It increases with M. This is in qualitative agreement with the results of the two-dimensional calculations of §3. Resulting from the worse resolution in the three-dimensional calculations, however, quantitatively there are slight differences ($\approx 5\%$) between the values from two-dimensional and three-dimensional results, respectively. The third curve, marked by triangles, shows $z_s(0)$, the maximum of the centre of u-distribution. As expected, the higher M is, the higher the M-shapedness measured by $z_s(0)$. It is due to the fact that with larger M, the blockage of the duct as discussed in the last section is higher, too.

The dashed curve seems to contradict this view. It shows the maximum of the transverse pressure difference $\Delta p_{t,\max}$ corresponding to the maximum difference between the two curves for pressure in figure 11. For convenience it is multiplied by ten. $\Delta p_{t,\max}$ decreases with M. Taking into account that the dimensional pressure results from multiplying the dimensionless one by M^2 (cf. §3.5), it is seen that the contradiction is only artificial.

The last, dotted curve shows the maximum transverse potential difference $\Delta\Phi_{t,\max}$. It is reached in the regions of fully developed MHD flow. The plot shows that it is independent of M. As the dimensional potential results from multiplying the dimensionless one by M, this agrees with physical intuition. The values shown for $\Delta\Phi_{t,\max}$ agree well with those of the two-dimensional calculations.

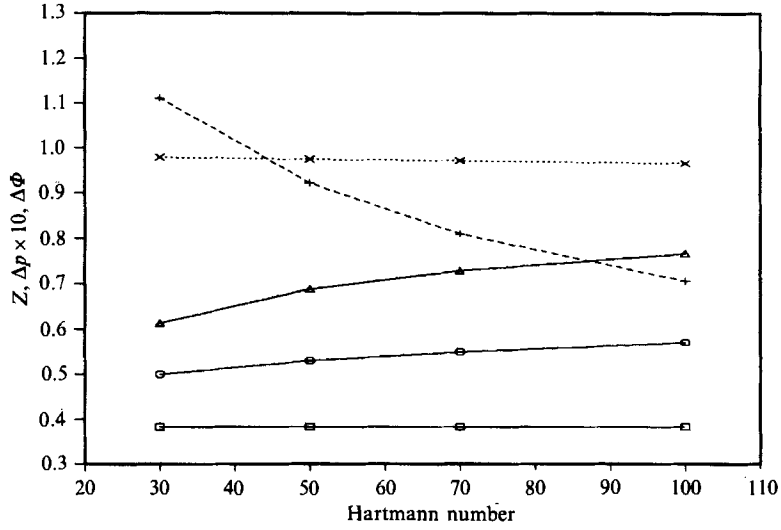

FIGURE 12. Dependence of three-dimensional effects on Hartmann number. □, centre of u-distribution, hydrodynamic; ○, centre of u-distribution, fully developed MHD; △, maximum centre of u-distribution; +, maximum transverse pressure difference ×10; ×, maximum transverse potential difference.

$c_t = c_b$	$c_l = c_r$	$z_{s,max}$	$z_{s,MHD}$	$\Delta p_{t,max}$	$\Delta\Phi_{t,max}$
0	0	0.7339	0.4327	0.0976	1.0390
10^{-3}	10^{-3}	0.7325	0.4359	0.0977	1.0381
0.1	10^{-3}	0.7118	0.5693	0.0960	1.0043
0.1	0.1	0.6889	0.5397	0.0923	0.9748
10^{-3}	1.0	0.6284	—	0.0732	0.8377

TABLE 1. Dependence of quantities characterizing three-dimensional MHD-flows in the region of variable magnetic field on wall conductance ratio.

Not shown is the behaviour of the same quantities as a function of x_0, the parameter governing the B-field gradient. As expected, the intensity of the three-dimensional effects decreases as x_0 increases thereby flattening the B_y-curve.

The three-dimensional phenomena are caused by electric currents. Because of this, the wall conductances are expected to influence them. Table 1 shows this influence with the aid of the maximum of the centre of u-distribution, $z_{s,max}$, the centre $z_{s,MHD}$ in fully developed MHD flow, the maximum transverse pressure difference $\Delta p_{t,max}$, and the maximum transverse potential difference $\Delta\Phi_{t,max}$.

As explained above, the three-dimensional effects are caused by currents flowing in the (x, z)-plane. These are influenced mainly by the conductivities c_l and c_r of the sidewalls. If the sidewalls are poorly conducting, the axial currents cannot enter them, but have to flow in the fluid. The relative difference between the Lorentz forces acting against the flow in the duct's centre and near the walls, is then greater than in the case of highly conducting walls. In that case, the currents can enter the walls, producing a large counter force in the side layers, too. If the sidewalls are poorly conducting, more current will flow parallel to $\boldsymbol{B}_0$ in the side layers, producing a smaller counter force, forcing more fluid into the side layers. The values shown for $z_{s,max}$ and $\Delta p_{t,max}$ confirm this view.

	$x_0 = 0.15$ (entrance)		$x_0 = -0.15$ (exit)	
N	$z_{s,\max}$	Δp_t	$z_{s,\max}$	$\Delta p_{t,\max}$
10^2	0.6835	0.1039	0.6626	0.1061
10^3	0.6889	0.0923	0.6911	0.0935
10^4	0.6911	0.0926	0.6914	0.0927

TABLE 2. Dependence of $z_{s,\mathrm{MHD}}$ and $\Delta p_{t,\max}$ on interaction parameter N and sign of x_0, i.e. begin or end of the magnetic field.

Unlike the three-dimensional effects in the transition region, the behaviour in the two-dimensional region is governed by currents in the (y, z) plane. Therefore the conductance ratios of all the walls are important, as can be seen from the corresponding values of table 1. For a deeper discussion compare §3.5.

The last parameter to be investigated is the interaction parameter N. As N describes inertia, it is reasonable here to discuss also the difference between flow into and out of a magnetic field, respectively. Therefore in table 2, the quantities $z_{s,\mathrm{MHD}}$ and $\Delta p_{t,\max}$ are displayed for $x_0 = 0.15$ as well as for $x_0 = -0.15$, for different N. As can easily be seen, inertia does not play a role for $N > 10^3$. Flow into and out of the field and cases between $N = 10^3$ and $N = 10^4$ are indistinguishable. The case $N = 10^2$, however, is different from those of higher N. Additionally, at $N = 10^2$ flows into and out of the field are different from one another. As inertia opposes the redistribution of the fluid, values for $z_{s,\max}$ are lower at $N = 10^2$ than at $N > 10^3$, indicating less M-shapedness. Since at the outlet from the field the strength of the Lorentz force decays, this effect is more pronounced there than at the inlet.

These observations are illustrated by figure 13 where the characteristic quantities known from figure 11 are plotted for two flows through a field ranging from about $x = -2$ to $x = +2$. The duct is non-conducting ($c = 0$) and the Hartmann number is 70. While in the upper plot, where $N = 10^3$, the beginning and end of the field region cannot be distinguished as they appear to be symmetric, the lower plot ($N = 10^2$) reveals non-symmetries between flow into and out of the field.

4.4.5. *Changes of c in streamwise direction, $c = c(x)$*

Unlike changes in the field strength, changes in the wall conductance ratio do not lead to significant three-dimensional effects. The transition between the two fully developed flows takes place monotonically and is confined to a small region. This is illustrated in figure 14 by the characteristic quantities for flow in a duct with a jump in wall conductivity. At $x = 0$, c jumps from 0.1 to 0.5. The magnetic field is constant everywhere. The reason for the absence of large three-dimensional effects is that only small axial currents are induced. As can be seen from the $\Delta\Phi_t$-curve in figure 14, the transverse potential differences are only slightly different in the two parts of the duct. This is in agreement with the values of $\Delta\Phi_{t,\max}$ at different c given in table 1. Therefore there is only a small axial potential difference driving only small currents. The Lorentz forces associated with them are not big enough to distort the flow.

4.4.6. *Flow channel insert*

In §3.5 it was shown that the longitudinal slot of an FCI has no influence on the flow if it is positioned at the sidewall. As the wall conductance ratios have only little effect on the three-dimensional phenomena in the region of variable magnetic field

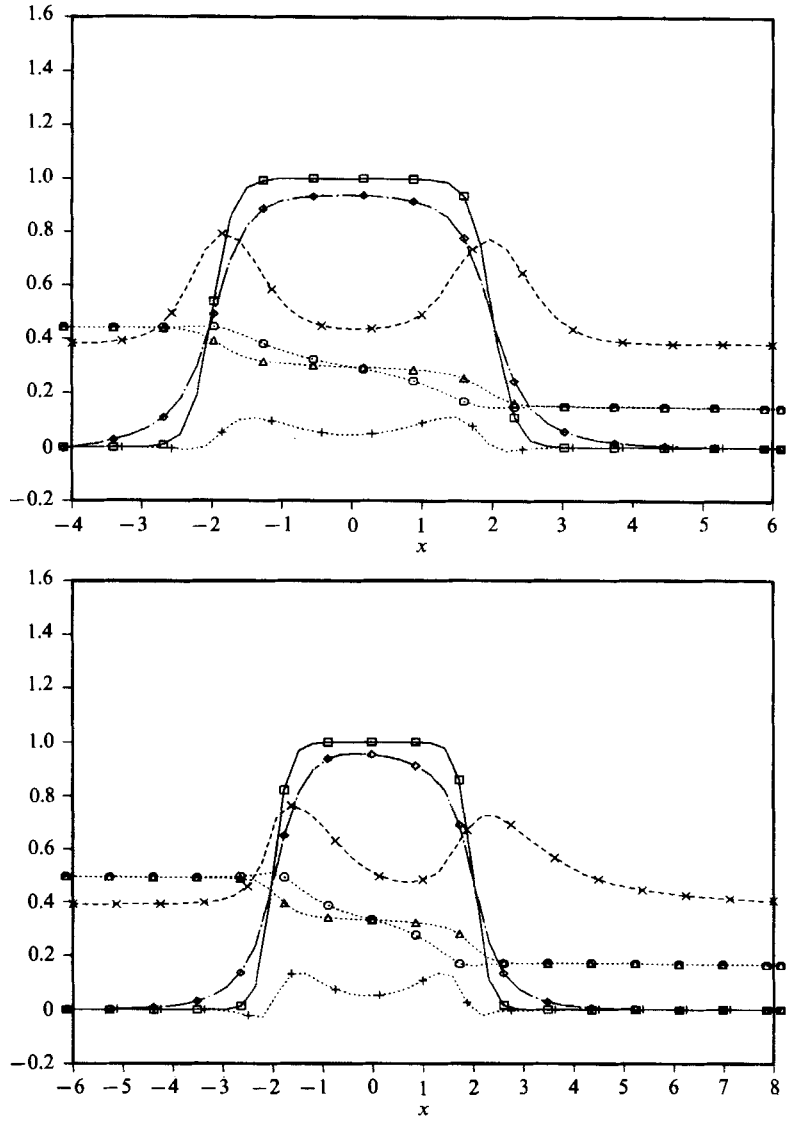

FIGURE 13. Characteristic quantities for flows traversing a magnet. $M = 70$ and $c = 0$. In the upper picture $N = 10^3$, entrance and exit appear symmetrical indicating that inertia does not play a role. In contrast to that, at $N = 10^2$ (lower picture), inertia influences the flow, as can be seen from the lack of symmetry between entrance and exit from the field. See figure 11 for key.

(cf. §4.4.4), the slot is expected to have only minor impact on the flow here. To confirm this expectation two calculations are performed, one with $c = 10^{-3}$ for all walls, the other with a small strip ($|y| \leqq 0.15$) of good conductance ($c = 0.1$) at the sidewall $z = 1$. The remaining parameters are $M = 50$, $N = 10^3$ and $x_0 = 0.15$. The overall pressure drop between $x = -4$ and $x = +4$ is $\Delta p = 0.2135$ in the first and $\Delta p = 0.2162$ in the second case. This is a very small difference. The slot produces only a small distortion in the boundary region of the velocity profile as shown in figure 15. It is concluded that the FCI fulfils its task in the variable field region also.

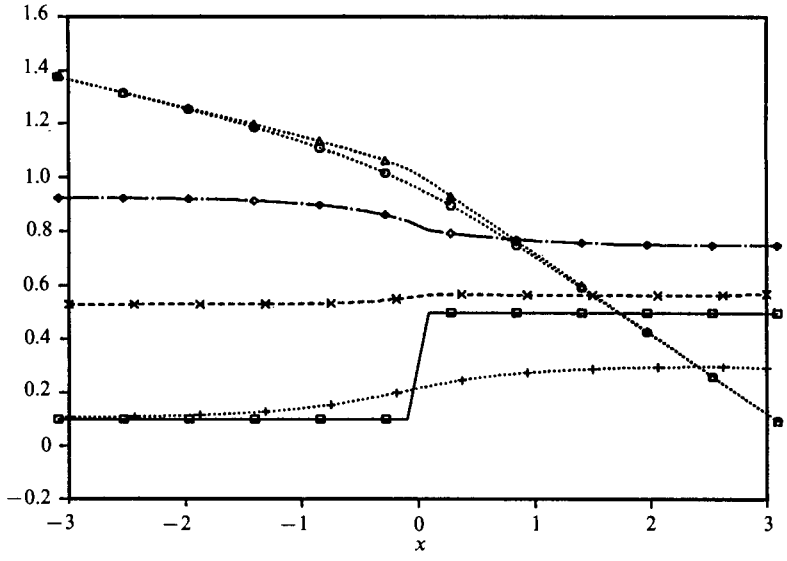

FIGURE 14. Characteristic quantities in a duct with a jump in wall conductivity as indicated by the solid curve. The magnetic field is homogeneous with $M = 50$ and $N = 10^3$. The transition takes place monotonically without leading to an M-shaped profile. □, Wall conductance ratio; other symbols as in figure 11.

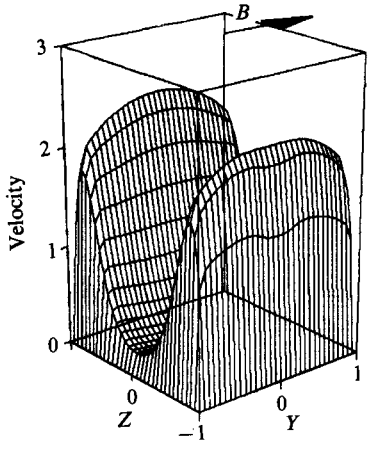

FIGURE 15. Influence of an FCI on the velocity profile in the region of increasing magnetic field strength. The profile shows a small distortion at the right wall where the well-conducting strip is situated. $x = 0.38$.

4.4.7. *Entrance length in an axial magnetic field*

Finally, we investigate the influence of an axially directed magnetic field, $B_x =$ constant, on the entrance length. At the entrance of the duct, the profile

$$u(x_1, y, z) = 1 + z, \quad v = w = 0, \tag{4.14}$$

is arbitrarily assumed, and the distance needed to reach fully developed flow is looked for, which in this case is identical to the purely hydrodynamic case.

The redistribution of the profile (4.14) requires motion perpendicular to the applied field B_x. As such a motion is suppressed by the field, the entrance length increases when M becomes larger, leading to a computational problem. For reasons

M	N	$Re = M^2/N$	x_E
50	10^3	2.5	5.7
50	10^2	25	6.9
100	10^2	100	> 16
Without	Field	100	7.6

TABLE 3. Entrance lengths x_E for different values of M and N at $c = 0$.

of capacity, the length of the computational domain cannot be made large enough for fully developed conditions to be really reached. The following measure for the entrance length is therefore chosen. The given profile at the entrance is non-symmetric in the z-direction, while the fully developed profile is symmetric. The deviation from symmetry can be used to judge the completeness of redistribution.

Symmetry is measured by the centre of u-distribution z_s^*, which is defined analogously to z_s of (4.12), except that the integrations now have to be performed over the full width of the duct. The fully developed profile is then characterized by $z_s^* = 0$. Since this value cannot be reached in the calculations as explained above, $z_s^* = 0.05$ is arbitrarily taken as the limit, and the entrance length x_E is defined to be the distance between entrance and the position where z_s^* reaches the value of 0.05.

Table 3 shows the entrance lengths x_E for different Hartmann numbers and interaction parameters in a duct with $c = 0$. For comparison, the value for a calculation without field is also given. It agrees well with values found in the literature, e.g. Zierep (1982), who for $Re = 100$ gives $x_E \approx 6$.

Comparing the entrance lengths for different sets of M and N, one can see that M influences x_E much more than N. As M measures the strength of the B-field, this observation agrees with the expectation that $\boldsymbol{B}$ suppresses motion perpendicular to itself.

5. Conclusion

Codes are developed for numerical simulation of two-dimensional as well as three-dimensional LMMHD flows. While in the two-dimensional case, flows with Hartmann numbers up to 10^3 are successfully calculated, the limit in the three-dimensional case is 10^2. These limits are due to the thin boundary layers governing MHD flow. These layers have to be resolved, leading to a large number of grid points. Thus storage is the crucial point. To reach higher Hartmann numbers as needed to predict performance of self-cooled fusion blankets, two ways are possible (*a*) to have bigger and faster machines using equidistant grids as in this work, (*b*) to use non-equidistant grids with many points in the thin layers and only a few in the core region. However, to best take advantage of the second approach, self-adjusting grids should be employed.

The results presented show how MHD flows are governed by the Lorentz force $\boldsymbol{j} \times \boldsymbol{B}$. Thus, to understand MHD flows, knowledge is needed about the electric currents induced in the fluid. They depend on the magnetic field and the conductivity of the walls. Besides raising the pressure losses, the Lorentz force produces velocity profiles with steep gradients at the wall. Among them are the M-shaped velocity profiles where the maximum velocity occurs in the side layers instead of at the duct's centre.

While the principles of MHD flows are known from earlier work (e.g. Hunt & Holroyd 1977; Holroyd & Walker 1978; Walker 1986*a*), the fully numerical

approach is able to remove the uncertainties arising from approximations or assumptions needed in analytical methods. Two examples are as follows.

(i) The comparison of pressure gradients obtained from the numerical calculations and the formula of Chang & Lundgren (1961), respectively, shows that the latter can be safely used for Hartmann numbers larger than 10 and non-conducting sidewalls.

(ii) The calculation of entrance lengths is an axially directed field directly yields the length of the transition region. It is much longer than in hydrodynamic flows, because redistribution of the flow requires motion perpendicular to the field, which is opposed by the currents induced.

However, the scope of this paper is not so much to present numbers for certain quantities of interest, but to show the ability of the numerical approach to calculate MHD flows and to provide a tool for their study. For instance, it is easily possible to change the boundary conditions to put electrodes into the walls or to manipulate the imposed field to include also an axial component.

The results of the calculations of flows in ducts with electrodes mainly confirm the work of Alty (1971), but for a certain configuration show a difference in the structure of the flow. In the case of short-circuited sidewalls and an angle between the horizontal and the field direction of less than 45°, Alty obtains thin jets extending parallel to the field lines from the corners to the opposite side walls. The calculations confirm the existance of these jets but show that they do not reach the opposite wall. The reason for this discrepancy is that Alty *a priori* assumes the variables to be constant along the field lines.

A topic of great interest is that of turbulence in MHD flows (e.g. Moffat 1967; Sommeria & Moreau 1982). However, with the present computer resources this problem cannot be solved. The values reached for the Hartmann and Reynolds numbers are not large enough for turbulence to occur. Accordingly, no kind of instability is found in the calculations performed.

This work has been performed in the framework of the Nuclear Fusion Project of the Kernforschungszentrum Karlsruhe and is supported by the European Communities within the European Fusion Technology Program.

I would like to thank Professor U. Müller for initiating this work and for his continuous interest in its progress. I gratefully acknowledge valuable discussions with Professor J. S. Walker, University of Illinois, concerning a general formulation of the boundary conditions.

REFERENCES

AITOV, T. N., KALYNTIK, A. I. & TANANAEV, A. V. 1983 Numerical analysis of three-dimensional MHD-flow in channels with abrupt change of cross section. *Magnetohydrodynamics* **19**, 223–229.

AITOV, T. N., KALYNTIK, A. I. & TANANAEV, A. V. 1984 Numerical study of three-dimensional MHD flow in a duct of complex configuration, using stokes approximation. *Magnetohydrodynamics* **20**, 288–293.

ALTY, C. J. N. 1971 Magnetohydrodynamic duct flow in a uniform transverse magnetic field of arbitrary orientation. *J. Fluid Mech.* **48**, 429–461.

ANDERSON, D. A., TANNEHILL, J. C. & PLETCHER, R. H. 1984 *Computational Fluid Mechanics and Heat Transfer*. McGraw-Hill.

BRILEY, W. R. & MCDONALD, H. 1980 On the structure and use of linearized block implicit schemes. *J. Comp. Phys.* **34**, 54–73.

CARRÉ, F., PROUST, E., REMOLOUV, J., RACABOY, A. & TILLIETTE, Z. 1984 Fusion Reactor Blanket – Comparative Evaluation Study. Rapport EMT/SERMA/BP/84/No. 584 T, 3591-21-000, January 17.

CHANG, C. C. & LUNDGREN, TH. S. 1961 Duct flow in magnetohydrodynamics. *Z. angew. Math. Phys.* **12**, 100–114.

DOUGLAS, J. & GUNN, J. E. 1964 A general formulation of alternating direction methods. Part 1. Parabolic and hyperpolic problems. *Num. Maths* **6**, 428–453.

HOLROYD, R. J. & MITCHELL, J. T. D. 1984 Liquid lithium as a coolant for tokamak fusion reactors. *Nucl. Engng Design/Fusion* **1**, 17–38.

HOLROYD, R. J. & WALKER, J. S. 1978 A theoretical study of the effects of wall conductivity, non-uniform magnetic fields and variable-area ducts on liquid-metal flows at high Hartmann number. *J. Fluid Mech.* **84**, 471–495.

HUA, T. Q. *et al.* 1988 Three dimensional MHD flows in rectangular ducts of liquid-metal-cooled blankets. *Fusion Tech.* **14**, 1389–1398.

HUA, T. Q. & PICOLOGLOU, B. F. 1989 Heat transfer in rectangular first wall coolant channels of liquid-metal cooled blankets. *Fusion Tech.* **15**, 1174.

HUNT, J. C. R. 1965 Magnetohydrodynamic flow in rectangular ducts. *J. Fluid Mech.* **21**, 577–590.

HUNT, J. C. R. 1969 A uniqueness theorem for magnetohydrodynamic duct flows. *Proc. Camb. Phil. Soc.* **65**, 319–327.

HUNT, J. C. R. & HOLROYD, R. J. 1977 Applications of laboratory and theoretical MHD duct flow studies in fusion reactor technology. UKAEA-Rep. CLM-R 169. (The results are also found in Holroyd & Walker 1978.)

KALIS, K. E. & TSINOBER, A. B. 1973 Numerical analysis of three dimensional MHD flow problems. *Magnetohydrodynamics* **2**, 35–40.

KHAN, S. 1987 Three-dimensional MHD entry flow in a duct with a laterally moving wall. *Arab. J. Sci. Engng* **12**, 405–412.

KHAN, S. & DAVIDSON, J. N. 1979 Magnetohydrodynamic coolant flows in fusion reactor blankets. *Ann. Nucl. Energy* **6**, 499–509.

KIM, J. & MOIN, P. 1985 Application of a fractional-step method to incompressible Navier–Stokes-Equations. *J. Comp. Phys.* **59**, 308–322.

MADARAME, M. & HAGIWARA, T. 1988 Computer code for analysing liquid metal MHD flow in rectangular ducts under strong transverse magnetic field. *First Intl Symp. on Fusion Nucl. Tech. Tokyo 1988*. To appear in *Fusion Engng Design*.

MALANG, S., ARHEIDT, K., BARLEON, L., BORGSTEDT, H. U., CASAL, V., FISCHER, U., LINK, W., REIMANN, J. & REUST, K. 1988 Self-cooled liquid-metal blanket concept. *Fusion Tech.* **14**, 1343–1356.

MOFFATT, H. K. 1967 On the suppression of turbulence by a uniform magnetic field. *J. Fluid Mech.* **28**, 571–592.

MOROZOVA, V. I., NAGORNYI, M. M. & ELKIN, A. J. 1983 Motion of a viscous, electrically conducting liquid through distributing and converging collectors in a transverse magnetic field. *Magnetohydrodynamics* **19**, 332–336.

PICOLOGLOU, B. F. 1985 Magnetohydrodynamic considerations for the design of self-cooled liquid-metal fusion reactor blankets. *Fusion Tech.* **8**, 276–282.

RAMOS, J. I. & WINOWICH, N. S. 1986 Magnetohydrodynamic channel flow study. *Phys. Fluid* **29**, S.992–997.

REED, C. B., PICOLOGLOU, B. F., HUA, T. Q. & WALKER, J. S. 1987 ALEX results – A comparison of measurements from a round and a rectangular duct with 3-D code predictions. *Proc. 12th Symp. on Fusion Engineering*, pp. 1267.

SCHUMANN, U. & SWEET, R. A. 1988 Fast Fourier transforms for direct solution of Poisson's equation with staggered boundary conditions. *J. Comp. Phys.* **75**, 123–137.

SEZGIN, M. 1987 Magnetohydrodynamic flow in a regular duct. *Intl. J. Num. Meth. Fluids* **7**, 697–718.

SMITH, D. L. *et al.* 1984 Blanket Comparison and Selection Study – Final Report, vol. 1–3, ANL/FPP-84-1, Sept. 1984.

SOMMERIA, J. & MOREAU, R. 1982 Why, how and when MHD turbulence becomes two-dimensional. *J. Fluid Mech.* **118**, 507–518.

STERL, A. 1989 Numerische Simulation magnetohydrodynamischer Flüssig-Metall-Strömungen in rechteckigen Rohren bei großen Harmannzahlen. Kernforschungszentrum Karlsruhe, KfK-4504.

SWARZTRAUBER, P. & SWEET, R. 1975 Efficient FORTRAN subprograms for the solution of elliptic partial differential equations. *NCAR Tech. Note* NCAR-LTN/IA-109.

TALMAGE, G. & WALKER, J. S. 1987 Three-dimensional laminar MHD-flow in ducts with thin metal walls and strong magnetic fields. *5th Beer-Sheva Seminar on MHD and Turbulence, Tel-Aviv.*

TEMPERLEY, D. J. 1984 Reconciliation of some discrepancies in results obtained for magnetohydrodynamic flow in a rectangular duct under an uniform transverse magnetic field at high Hartmann number. *Arch. Mech.* **35**, (5–6), 673–686.

THOMPSON, J. F. 1985 A survey of dynamically-adaptive grids in the numerical solution of partial differential equations. *Appl. Maths* **1**, 3–27.

TILLACK, M. S. 1988 Examination of MHD fluid flow in geometric elements of a fusion reactor blanket using the core flow approach. *First Intl Symp. on Fusion Nucl. Techn. Tokyo 1988.* To appear in *Fusion Engng Design.*

WALKER, J. S. 1981 Magnetohydrodynamic flows in rectangular ducts with thin conducting walls. Part I: Constant area and variable area ducts with strong uniform magnetic fields. *J. Méc.* **20**, 79–112.

WALKER, J. S. 1986*a* Laminar duct flows in strong magnetic fields. In *Liquid-Metal Flows and Magnetohydrodynamics*, vol. 2 (ed. H. Branover, P. S. Lykoudis & M. Moon), pp. 3–16. American Institute of Aeronautics and Astronautics, New York.

WALKER, J. S. 1986*b* Liquid-metal MHD flow in a duct whose cross section changes from a rectangle to a trapezoid, with applications in fusion blanket design. *Argonne Nat. Lab. Rep.* ANL/FPP/TM-206.

WALKER, J. S. 1986*c* Liquid-metal MHD flow in a thin conducting pipe near the end of a uniform magnetic field. *J. Fluid Mech.* **167**, S.199–217. *Argonne Nat. Lab. Rep.* ANL/FPP/TM-205.

WALKER, J. S. 1986*d* Liquid-metal flow in a rectangular duct with a non-uniform magnetic field. *Argonne Nat. Lab. Rep.* ANL/FPP/TM-207.

WALKER, J. S. 1986*e* Liquid-metal flow through a thin-walled elbow in a plane perpendicular to a uniform magnetic field. *Argonne Nat. Lab. Rep.* ANL/FPP/TM-204, *Intl J. Engng Sci.* **24**, 1741–54.

WALKER, J. S. & LUDFORD, G. S. S. 1974*a* MHD flow in conducting circular expansions with strong transverse magnetic fields. *Intl J. Engng Sci.* **12**, 193–204.

WALKER, J. S. & LUDFORD, G. S. S. 1974*b* MHD flow in insulated circular expansions with strong transverse magnetic fields. *Intl J. Engng Sci.* **12**, 1045–1061.

WALKER, J. S. & LUDFORD, G. S. S. 1975 MHD flow in circular expansions with thin conducting walls. *Intl J. Engng Sci.* **13**, 261–269.

WINOWICH, N. S. & HUGHES, W. F. 1982 A finite element analysis of two-dimensional MHD-flows. In *Liquid Metal Flows and MHD* (ed. M. Branover, P. S. Lykoudis & A. Yakhot). 3rd Intl Sem. in the MHD and Turbulence Series, Beer Sheva, 1981, Am. Inst. of Aeronautics and Astronautics, 1982.

WU, S. T. 1973 Unsteady MHD duct flow by the finite element method. *Intl J. Num. Math. Engng.* **6**, S.3–10.

YAGAWA, G. & MASUDA, M. 1982 Finite element analysis of magnetohydrodynamics and its application to lithium blanket design of a fusion reactor. *Nucl. Engng Design* **71**, 121–136.

ZIEREP, J. 1982 Grundzüge der Strömungslehre, 2nd edn. Karlsruhe.